Journal of Advanced Ceramics
2020, **9**(5): 588–594
https://doi.org/10.1007/s40145-020-0397-2
ISSN 2226-4108
CN 10-1154/TQ

Research Article

Effect of Sb-site nonstoichiometry on the structure and microwave dielectric properties of $Li_3Mg_2Sb_{1-x}O_6$ ceramics

Cuijin PEI[a], Jingjing TAN[a], Yang LI[a], Guoguang YAO[a,b,*], Yanmin JIA[a], Zhaoyu REN[b], Peng LIU[c], Huaiwu ZHANG[d]

[a]*School of Science, Xi'an University of Posts and Telecommunications, Xi'an 710121, China*
[b]*School of Physics, Northwest University, Xi'an 710069, China*
[c]*College of Physics and Information Technology, Shaanxi Normal University, Xi'an 710062, China*
[d]*State Key Laboratory of Electronic Thin Films and Integrated Devices, University of Electronic Science and Technology of China, Chengdu 610054, China*

Received: January 14, 2020; Revised: May 31, 2020; Accepted: June 13, 2020

Abstract: The non-stoichiometric $Li_3Mg_2Sb_{1-x}O_6$ ($0.05 \leqslant x \leqslant 0.125$) compounds have been prepared via the mixed oxide method. The influences of Sb nonstoichiometry on the sintering behavior, microstructure, phase composition along with microwave dielectric performances for $Li_3Mg_2Sb_{1-x}O_6$ ceramics were studied. Combined with X-ray diffraction (XRD) and Raman spectra, it was confirmed that phase composition could not be affected by the Sb nonstoichiometry and almost pure phase $Li_3Mg_2SbO_6$ was formed in all compositions. Appropriate Sb-deficiency in $Li_3Mg_2SbO_6$ not only lowered its sintering temperature but also remarkably improved its $Q\times f$ value. In particular, non-stoichiometric $Li_3Mg_2Sb_{0.9}O_6$ ceramics sintered at 1250 ℃/5 h owned seldom low dielectric constant $\varepsilon_r = 10.8$, near-zero resonant frequency temperature coefficient $\tau_f = -8.0$ ppm/℃, and high quality factor $Q\times f$ = 86,300 GHz (at 10.4 GHz). This study provides an alternative approach to ameliorate its dielectric performances for $Li_3Mg_2SbO_6$-based compounds through defect-engineering.

Keywords: microwave dielectric properties; ceramics; sintering; antimony compounds

1 Introduction

Nowadays, the high-speed advancement in the 5th-generation communication industry has prompted a massive demand for dielectric materials owning outstanding dielectric properties in the high-frequency region [1]. To satisfy the particular criteria, the microwave dielectric material must own following essential parameters: low dielectric constant (ε_r) to shorten signal transition time, small resonant frequency temperature coefficient (τ_f) to enhance thermal stabilization, and high quality factor ($Q\times f$) or low dielectric loss to enhance frequency selectivity [2]. It is still a challenge for one material owing ε_r, τ_f, and $Q\times f$ simultaneously since the majority of microwave dielectric ceramics commonly own low ε_r but large negative τ_f values [3]. To obtain near-zero τ_f, one effective approach is to prepare a solid solution or composite ceramics [4]. However, this method could usually deteriorate the host ceramics' microwave dielectric properties to some extent owing to the unexpected secondary phase or ion

* Corresponding author.
E-mail: yaoguoguang@xupt.edu.cn

diffusion [5,6]. Therefore, new material systems owing above parameters simultaneously need to be explored and investigated [7].

In 1982, Castellanos *et al*. [8] reported an orthorhombic $Li_3Mg_2SbO_6$ (LMS) compound. Recently, the LMS compound has received much attention due to its potential application in fields such as luminescence and microwave dielectric materials [9–13]. Zhang *et al*. [13] reported the microwave dielectric properties of $Li_3Mg_2(Nb_{1-x}Sb_x)O_6$ ($0.02 \leqslant x \leqslant 0.08$) ceramics. We firstly reported the microwave dielectric performances ($Q\times f$ = 49,000 GHz, τ_f = –18.0 ppm/℃) of nominal composition LMS ceramics prepared with a mixed oxide method [9]. Yet its poor sinterability (dehiscence) and low $Q\times f$ inhibit its practical application, which is connected with the secondary phase SbO_x [9]. Lately, we doped modified solid-state reaction method, which not only effectively suppressed the secondary phase SbO_x but also improved the sinterability and dielectric characterizations of LMS ceramics [10]. The above-modified process not only prolongs the preparation period, but also enhances the cost. Recently, many researchers have demonstrated that the sintering behavior and dielectric performances can be ameliorated through introducing non-stoichiometric composition in some material systems [14–17]. However, the effects of non-stoichiometry on $Li_3Mg_2SbO_6$ ceramics have not yet been reported. In the current paper, the influences of Sb-site nonstoichiometry on the sintering behavior, phase constitution combined with microwave dielectric characterizations of $Li_3Mg_2Sb_{1-x}O_6$ compounds have been studied.

2 Experimental

The non-stoichiometric $Li_3Mg_2Sb_{1-x}O_6$ ($0.05 \leqslant x \leqslant 0.125$) were synthesized via solid-state ceramics processing. The reagents of Sb_2O_3 (99.0%, Guo-Yao Co., Ltd., Shanghai, China), MgO (99.99%, Mountain Development Center, Beijing, China), and Li_2CO_3 (98.0%, Guo-Yao Co., Ltd., Shanghai, China) were used as staring materials. According to non-stoichiometric $Li_3Mg_2Sb_{1-x}O_6$, the corresponding raw materials were weighed and ground for 8 h using ZrO_2 balls as well as absolute ethanol as media. The resultant milled powders were roasted under 80 ℃/5 h, and calcined at 900 ℃/4 h. After second ball-milled for 8 h, the ball-milled powders were mixed with 6% polyvinyl alcohol solution as the binder, and then granulated manually. The granules were pressed into cylindrical pucks (Φ10 mm × 6 mm) under 200 MPa. After debinding at 500 ℃ for 2 h, the pucks were fired under 1200–1275 ℃ dwelling for 5 h.

The phase constitutions of samples have been characterized using X-ray diffraction (XRD, RigakuD/MAX2550, Tokyo, Japan) with Cu Kα radiation and Raman spectra (Jobin Yvon, Longjumeau, France) equipped with He–Ne laser (633 nm) and an output of 30 mW. X-ray photoelectron spectroscopy (XPS) measurement was carried out with a spectrometer (Axis Ultra, UK) using Al Ka (1486.6 eV) radiation. The surface morphology of sintered bodies was analyzed by adopting scanning electron microscope (SEM, Hitachi, Tokyo, Japan). The bulk densities of sintered bodies were evaluated based on Archimedes' principle. The ε_r and $Q\times f$ values of samples were tested through vector network analyzer (N5230A, Agilent, America) under about 10–12 GHz. The τ_f value for samples was calculated by Eq. (1):

$$\tau_f = \frac{(f_2 - f_1)\times 10^6}{f_1 \times (85-25)} \quad (1)$$

where f_1 and f_2 denote the measured frequencies under 25 and 85 ℃, respectively.

3 Results and discussion

The refined XRD patterns and refinement parameters for $Li_3Mg_2Sb_{1-x}O_6$ ($0.05 \leqslant x \leqslant 0.125$) specimens heated at 1250 ℃ are displayed in Fig. 1 and Table 1, respectively. As shown in Fig. 1, the calculated XRD profiles based on $Li_3Co_2TaO_6$ (ICSD #81043) structural model matched well with those of experimental ones. It indicated that for all compositional specimens, almost pure phase $Li_3Mg_2SbO_6$ was formed along with trace amount of unknown phase (marked as * in Fig. 1), although the maximum 12.5 mol% Sb-site defects were introduced. Similar phenomena were also reported in other materials [18]. In addition, as seen in Table 1, the cell volume was enlarged when x increased from 0.05 to 0.125, which is due to the increased concentration of V_o caused by Sb^{5+} ion defects [19,20]. Figure 2 gives the refined XRD plots for $Li_3Mg_2Sb_{0.9}O_6$ specimens heated at 1200–1275 ℃. No obvious phase constitution change or peak position shift was observed in Fig. 2, which indicated that there was no obvious change

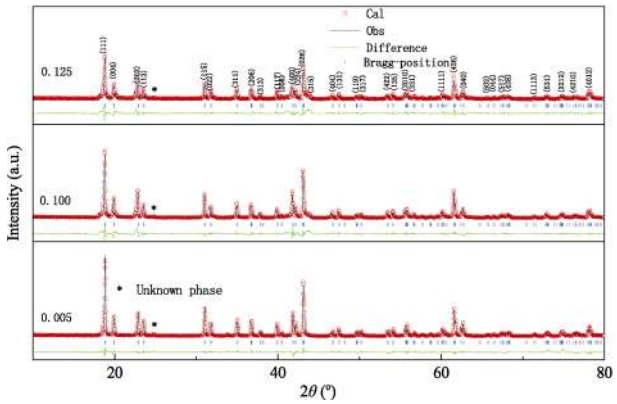

Fig. 1 Refined XRD patterns of $Li_3Mg_2Sb_{1-x}O_6$ ceramics sintered at 1250 ℃.

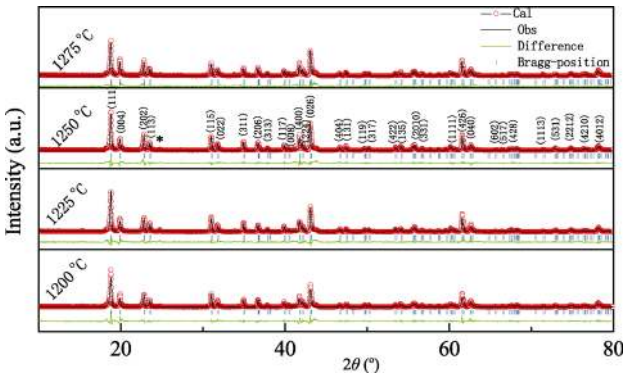

Fig. 2 Refined XRD patterns of $Li_3Mg_2Sb_{0.9}O_6$ ceramics under different sintering temperatures.

Table 1 Refinement parameters and reliability factors of $Li_3Mg_2Sb_{1-x}O_6$ ceramics sintered at 1250 ℃ for 5 h

x	a (Å)	b (Å)	c (Å)	Cell volume (Å^3)	R_p (%)	R_{wp} (%)
0.05	8.6292	5.9265	17.7958	910.0941	10.23	14.81
0.10	8.6409	5.9324	17.7829	911.5741	9.21	12.91
0.125	8.6409	5.9403	17.7712	912.1875	10.08	13.74

of unit cell volume. Therefore, based on the definition of packing fraction [21], there should be no change of packing fraction regardless of sintering temperature for a given composition. Compared to Ref. [9], the secondary phase in $Li_3Mg_2SbO_6$-based ceramics could be effectively inhibited by introduced partial Sb-site deficiency within the crystals.

The typical Raman spectra of $Li_3Mg_2Sb_{1-x}O_6$ samples under different sintering temperatures are depicted in Fig. 3. Only three Raman peaks (475, 551, and 655 cm^{-1}) are present in all samples, which are similar to the characteristic Raman spectra of $Li_3Mg_2SbO_6$ [10]. The Raman peak at 655 cm^{-1} can attribute to the asymmetric stretching vibration of Sb–O–Sb bond in SbO_6 octahedral. The Raman peaks at 551 and 475 cm^{-1} are associated with the Li/Mg–O bonds vibration. In addition, there was no significant change of Raman shifts and Raman peak intensity under different sintering temperatures, which were associated with inherent microwave dielectric properties [22]. Furthermore, the Raman band of SbO_6 octahedron (655 cm^{-1}) slightly shifted to lower frequency with increasing x content as seen the inset in Fig. 3. According to Refs. [15,23], the Raman shift of SbO_6 octahedron depended mainly on the Sb–O bond: $\upsilon = 21349\exp(-1.9176 d_{Sb-O})$, where υ and d_{Sb-O} represent Raman shift and Sb–O bond length, respectively. This indicated that the Raman shift was inversely proportional to the unit cell volume. Therefore, the Raman analysis confirmed that the unit cell volume of $Li_3Mg_2Sb_{1-x}O_6$ ceramics expand with increasing x content, which was well correlated with the XRD results.

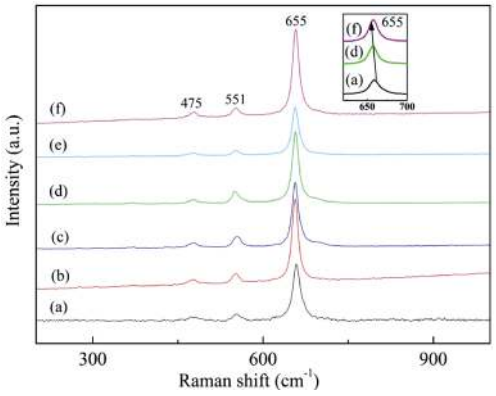

Fig. 3 Characteristic Raman spectra of $Li_3Mg_2Sb_{1-x}O_6$ ceramics fired under various temperatures: (a) $Li_3Mg_2Sb_{0.95}O_6$, 1250 ℃, (b) $Li_3Mg_2Sb_{0.9}O_6$, 1200 ℃, (c) $Li_3Mg_2Sb_{0.9}O_6$, 1225 ℃, (d) $Li_3Mg_2Sb_{0.9}O_6$, 1250 ℃, (e) $Li_3Mg_2Sb_{0.9}O_6$, 1275 ℃, and (f) $Li_3Mg_2Sb_{0.875}O_6$, 1250 ℃.

Figure 4 exhibits the SEM photographs of polished and thermally etched surfaces for $Li_3Mg_2Sb_{1-x}O_6$ samples heated under different temperatures. As seen from Figs. 4(a) and 4(e), a relatively porous structure was observed for $Li_3Mg_2Sb_{0.9}O_6$ fired at 1200 ℃ and for $Li_3Mg_2Sb_{0.95}O_6$ fired at 1250 ℃, respectively. As seen from Figs. 4(a)–4(c), the amount of pores are alleviated, and mean grain size is promoted with the increment temperature. The 1250 ℃-sintered specimen (Fig. 4(c)) exhibited a dense microstructure, implying a higher dielectric performance [24]. However, for $Li_3Mg_2Sb_{0.9}O_6$ fired at 1275 ℃ and $Li_3Mg_2Sb_{0.875}O_6$ sintered at 1250 ℃, anomalous grain growth along with pores appeared due to over-sintering, which would deteriorate the performances of samples [25]. Table 2 lists

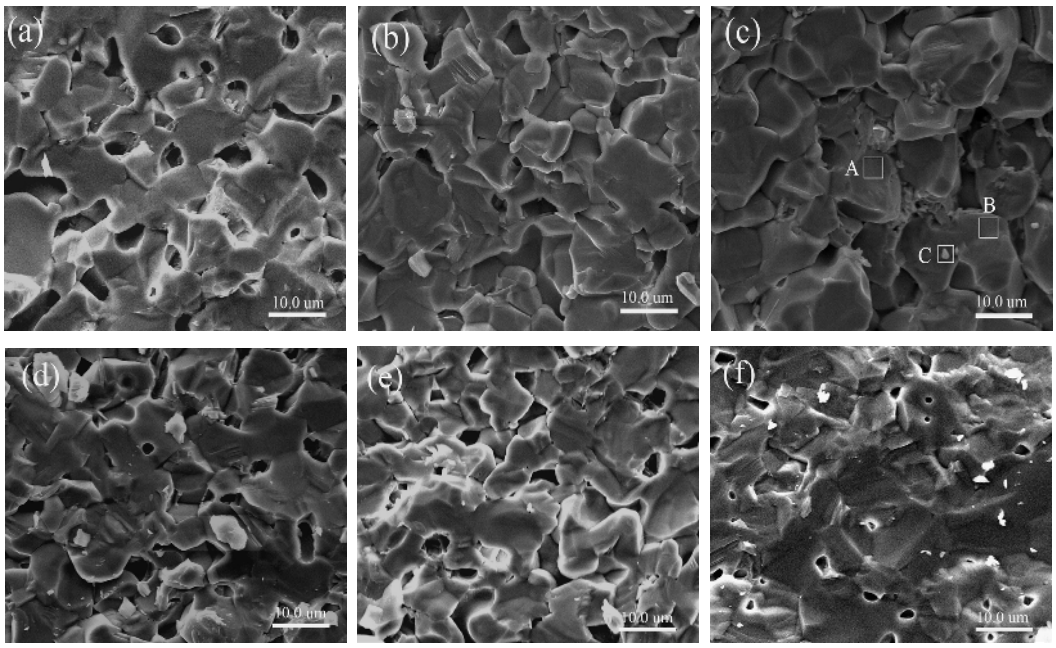

Fig. 4 Typical SEM photographs of polished and thermally etched surfaces for $Li_3Mg_2Sb_{1-x}O_6$ ceramics under different firing temperatures: (a) $Li_3Mg_2Sb_{0.9}O_6$, 1200 ℃, (b) $Li_3Mg_2Sb_{0.9}O_6$, 1225 ℃, (c) $Li_3Mg_2Sb_{0.9}O_6$, 1250 ℃, (d) $Li_3Mg_2Sb_{0.9}O_6$, 1275 ℃, (e) $Li_3Mg_2Sb_{0.95}O_6$, 1250 ℃, and (f) $Li_3Mg_2Sb_{0.875}O_6$, 1250 ℃.

Table 2 Energy disperse spectroscopy (EDS) data of the grains A–C marked in Fig. 4(c)

Grain	Weight (wt%)			Atom (wt%)		
	MgK	SbL	OK	MgK	SbL	OK
A	22.07	50.55	27.37	29.93	13.69	56.39
B	23.00	47.40	29.61	29.69	12.22	58.09
C	25.86	37.30	36.84	28.96	08.34	62.69

the concentrations of compositional elements, which were conducted on grains A–C marked in Fig. 4(c) by the EDS analysis. The EDS analysis revealed that the constitution of large grains (marked A and B) is $Li_3Mg_2SbO_6$, whereas the smaller and brighter grains are enriched in Mg (marked C). This is consistent with XRD results.

Figure 5 shows the bulk density of $Li_3Mg_2Sb_{1-x}O_6$ ceramics after heat treatment at 1200–1275 ℃. For $Li_3Mg_2Sb_{0.95}O_6$ sample, the bulk density gradually increased with increasing temperature from 1200 to 1275 ℃, indicating it has high densification sintering temperature. However, for $Li_3Mg_2Sb_{0.9}O_6$ sample, the bulk density increased gradually to the maximum at 1250 ℃ and subsequently descended. The enhancement in bulk density of $Li_3Mg_2Sb_{0.9}O_6$ sample could attribute to the reduction in porosity and grain boundaries, whereas its decrement could attribute to the anomalous grain growth, as displayed in Fig. 4. In addition, compared with $Li_3Mg_2SbO_6$ ceramics [10], the low sintering temperature of $Li_3Mg_2Sb_{0.9}O_6$ ceramics

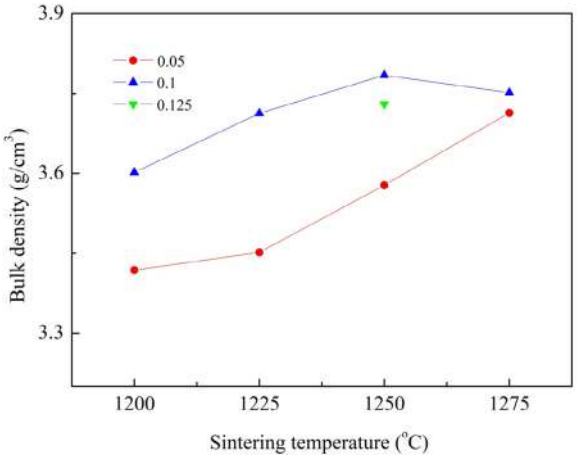

Fig. 5 Bulk density of $Li_3Mg_2Sb_{1-x}O_6$ ceramics following sintered at 1200–1275 ℃.

could attribute to the Sb deficiency and oxygen vacancies within the crystals [26].

Figure 6 displays the variations in ε_r, τ_f, and $Q\times f$ of $Li_3Mg_2Sb_{1-x}O_6$ compounds with firing temperature. In general, ε_r is dramatically dependent on density, ionic polarizability, secondary phase, etc. [27]. The relationship between ε_r and sintering temperature or composition of $Li_3Mg_2Sb_{1-x}O_6$ ceramics revealed a similar tendency as between density and sintering temperature or composition, as shown in Fig. 6(a). Thus, the ε_r value is mainly influenced by densification rather than ionic polarizability and secondary phase. In addition, the τ_f values of

$Li_3Mg_2Sb_{0.9}O_6$ ceramics remained stable (about –8.0 ppm/℃) regardless of sintering temperatures as seen in Fig. 6(b). Both intrinsic parameters (vibration modes and packing fraction) and extrinsic parameters (density, mean grain size, phase composition, etc.) can influence the $Q\times f$ value of ceramics [28,29]. In the present ceramics, the intrinsic factors should be ignored because of no significant change of vibration mode (Fig. 3) and packing fraction as mentioned before. As illustrated in Fig. 6(c), when firing temperature varied from 1200 to 1250 ℃, the $Q\times f$ value of specimens gradually enhanced and obtained a maximum value of ~62,800 GHz for $Li_3Mg_2Sb_{0.95}O_6$ at 1250 ℃, and ~86,300 GHz for $Li_3Mg_2Sb_{0.9}O_6$ at 1250 ℃, respectively. The increased densification and average grain size could be responsible for the improvement of $Q\times f$ value [30]. Beyond this temperature, their $Q\times f$ values decreased slightly, which may be connected with the anomalous grain growth [25]. Interestingly, the $Li_3Mg_2Sb_{0.875}O_6$ ceramics sintered below 1250 ℃ showed poor resonance, which was due to the effect of the yellow core caused by the valence change of antimony ions (Fig. 7) [31]. The resemble phenomena have also been observed in Ti-containing oxides ceramics [32,33]. However, the $Li_3Mg_2Sb_{0.875}O_6$ sample sintered at 1250 ℃ exhibited $Q\times f \approx$ 37,400 GHz due to the absence of yellow cores. A more detailed explanation about this phenomenon is expected in further research. At a given sintering temperature of 1250 ℃, the $Li_3Mg_2Sb_{0.9}O_6$ sample exhibited superior $Q\times f$ value than the others, indicating moderate Sb-deficiency is benefited to improve the $Q\times f$ value of $Li_3Mg_2SbO_6$-based ceramics. The true reason is still unknown and further research is in progress. Compared to our previous study [10], the non-stoichiometric $Li_3Mg_2Sb_{0.9}O_6$ ceramics fabricated by classical solid-state method owned comparable dielectric performances with $Li_3Mg_2SbO_6$ ceramics prepared via modified two-stage process, but relatively lower sintering temperature and simple synthesis process. The comparable or even slightly enhanced $Q\times f$ value would be related to the distortion of crystal lattice caused by an appropriate Sb-site nonstoichiometry, a similar phenomenon was also reported in other ceramic systems [34–36]. Moreover, the $Q\times f$ value (86,300 GHz, at 10.4 GHz) of $Li_3Mg_2Sb_{0.9}O_6$ ceramics is 1.7 times larger than that of nominal composition $Li_3Mg_2SbO_6$ ceramics ($Q\times f$ = 49,000 GHz at 11.0 GHz), which is ascribed to the absence of secondary SbO_x [9].

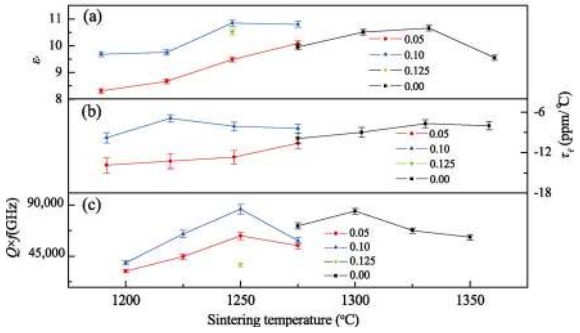

Fig. 6 Variations in microwave dielectric properties of $Li_3Mg_2Sb_{1-x}O_6$ ceramics under different firing temperatures.

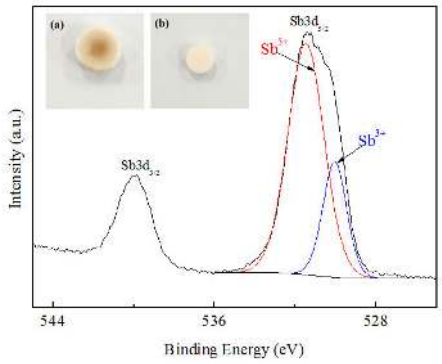

Fig. 7 Sb 3d region of XPS spectra of 1225 ℃-sintered $Li_3Mg_2Sb_{0.875}O_6$. The inset illustrates the evidence of coring in $Li_3Mg_2Sb_{0.875}O_6$ samples fired at different conditions: (a) 1225 and (b) 1250 ℃.

4 Conclusions

The non-stoichiometric $Li_3Mg_2Sb_{1-x}O_6$ ($0.05 \leqslant x \leqslant 0.125$) ceramics were fabricated, and their phase composition, sintering character, and dielectric properties were characterized. XRD and Raman spectrum results confirmed that $Li_3Mg_2SbO_6$ without obvious secondary phase can be maintained within the compositional range of $0.05 \leqslant x \leqslant 0.125$. The sinterability and $Q\times f$ values were tremendously improved by introducing appropriate Sb-deficiency in $Li_3Mg_2SbO_6$. Especially, the nonstoichiometric $Li_3Mg_2Sb_{0.9}O_6$ ceramics sintered at 1250 ℃ simultaneously exhibited small τ_f of –8.0 ppm/℃ and ε_r of 10.8, a high $Q\times f$ of 86,300 GHz (at 10.4 GHz). The favorable combined microwave dielectric performances make it an alternative material for millimeter-wave devices.

Acknowledgements

The authors acknowledge the support from the National

Natural Science Foundation of China (Grant No. 51402235), China Postdoctoral Science Foundation (2015M582696), Science and Technology Plan Project of Xi'an Bureau of Science and Technology (GXYD17.19), Education Department of Shaanxi Province (18JK0711), and Innovation Funds of Graduate Programs of Xi'an University of Posts and Telecommunications (CXJJLD2019020).

References

[1] Zhang X, Tang B, Fang ZX, *et al*. Structural evolution and microwave dielectric properties of a novel $Li_3Mg_{2-x/3}Nb_{1-2x/3}Ti_xO_6$ system with a rock salt structure. *Inorg Chem Front* 2018, **5**: 3113–3125.

[2] Zhang YH, Sun JJ, Dai N, *et al*. Crystal structure, infrared spectra and microwave dielectric properties of novel extra low-temperature fired $Eu_2Zr_3(MoO_4)_9$ ceramics. *J Eur Ceram Soc* 2019, **39**: 1127–1131.

[3] Reaney IM, Iddles D. Microwave dielectric ceramics for resonators and filters in mobile phone networks. *J Am Ceram Soc* 2006, **89**: 2063–2072.

[4] Gu FF, Chen GH, Li XQ, *et al*. Structural and microwave dielectric properties of the $(1-x)Li_3NbO_4$–$xCa_{0.8}Sr_{0.2}TiO_3$ thermally stable ceramics. *Mater Chem Phys* 2015, **167**: 354–359.

[5] Zou ZY, Chen ZH, Lan XK, *et al*. Weak ferroelectricity and low-permittivity microwave dielectric properties of $Ba_2Zn_{(1+x)}Si_2O_{(7+x)}$ ceramics. *J Eur Ceram Soc* 2017, **37**: 3065–3071.

[6] Dong MZ, Yue ZX, Zhuang H, *et al*. Microstructure and microwave dielectric properties of TiO_2-doped Zn_2SiO_4 ceramics synthesized through the sol-gel process. *J Am Ceram Soc* 2008, **91**: 3981–3985.

[7] Huang CL, Tseng YW. Structure, dielectric properties, and applications of $CaTiO_3$-modified $Ca_4MgNb_2TiO_{12}$ ceramics at microwave frequency. *J Am Ceram Soc* 2011, **94**: 1824–1828.

[8] Castellanos M, Gard JA, West AR. Crystal data for a new family of phases, $Li_3Mg_2XO_6$: X = Nb, Ta, Sb. *J Appl Cryst* 1982, **15**: 116–119.

[9] Yao GG, Pei CJ, Gong Y, *et al*. Microwave dielectric properties of temperature stable $(1-x)Li_3Mg_2SbO_6$–$xBa_3(VO_4)_2$ composite ceramics. *J Mater Sci: Mater Electron* 2018, **29**: 9979–9983.

[10] Pei CJ, Hou CD, Li Y, *et al*. A low ε_r and temperature-stable $Li_3Mg_2SbO_6$ microwave dielectric ceramics. *J Alloys Compd* 2019, **792**: 46–49.

[11] Wang SY, Sun Q, Devakumar B, *et al*. Mn^{4+}-activated $Li_3Mg_2SbO_6$ as an ultrabright fluoride-free red-emitting phosphor for warm white light-emitting diodes. *RSC Adv* 2019, **9**: 3429–3435.

[12] Zhong JS, Chen X, Chen DQ, *et al*. A novel rare-earth free red-emitting $Li_3Mg_2SbO_6$: Mn^{4+} phosphor-in-glass for warm w-LEDs: Synthesis, structure, and luminescence properties. *J Alloys Compd* 2019, **773**: 413–422.

[13] Zhang P, Wu SX, Xiao M. Effect of Sb^{5+} ion substitution for Nb^{5+} on crystal structure and microwave dielectric properties for $Li_3Mg_2NbO_6$ ceramics. *J Alloys Compd* 2018, **766**: 498–505.

[14] Guo WJ, Zhang J, Luo Y, *et al*. Microwave dielectric properties and thermally stimulated depolarization of Al-doped $Ba_4(Sm,Nd)_{9.33}Ti_{18}O_{54}$ ceramics. *J Am Ceram Soc* 2019, **102**: 5494–5502.

[15] Li B, Zheng JG, Li W. Enhanced effect of vanadium ions non-stoichiometry on microwave dielectric properties of $Ca_5Co_4V_{6+x}O_{24}$ ceramics. *Mater Chem Phys* 2018, **207**: 282–288.

[16] Belous A, Ovchar O, Jancar B, *et al*. The effect of non-stoichiometry on the microstructure and microwave dielectric properties of the columbites $A^{2+}Nb_2O_6$. *J Eur Ceram Soc* 2007, **27**: 2933–2936.

[17] Li JM, Fan CG, Cheng ZX, *et al*. Influence of Zn nonstoichiometry on the phase structure, microstructure and microwave dielectric properties of $Nd(Zn_{0.5}Ti_{0.5})O_3$ ceramics. *J Alloys Compd* 2019, **793**: 385–392.

[18] Pang LX, Zhou D, Yue ZX. Temperature independent low firing $[Ca_{0.25}(Nd_{1-x}Bi_x)_{0.5}]MoO_4$ ($0.2 \leqslant x \leqslant 0.8$) microwave dielectric ceramics. *J Alloys Compd* 2019, **781**: 385–388.

[19] Pan WG, Cao MH, Qi JL, *et al*. Defect structure and dielectric behavior in $SrTi_{1-x}(Zn_{1/3}Nb_{2/3})_xO_3$ ceramics. *J Alloys Compd* 2019, **784**: 1303–1310.

[20] Muhammad R, Khesro A. Influence of A-site nonstopichiometry on the electrical properties of BT-BMT. *J Am Ceram Soc* 2017, **100**: 1091–1097.

[21] Kim ES, Chun BS, Freer R, *et al*. Effects of packing fraction and bond valence on microwave dielectric properties of $A^{2+}B^{6+}O_4$ (A^{2+}:Ca,Pb,Ba; B^{6+}:Mo,W) ceramics. *J Eur Ceram Soc* 2010, **30**: 1731–1736.

[22] Wang Y, Tang TL, Zhang JT, *et al*. Preparation and microwave dielectric properties of new low-loss $NiZrTa_2O_8$ ceramics. *J Alloys Compd* 2019, **778**: 576–578.

[23] Hardcastle FD, Wachs IE. Determination of molybdenum-oxygen bond distances and bond orders by Raman spectroscopy. *J Raman Spectrosc* 1990, **21**: 683–691.

[24] Wu SP, Chen DF, Jiang C, *et al*. Synthesis of monoclinic $CaSnSiO_5$ ceramics and their microwave dielectric properties. *Mater Lett* 2013, **91**: 239–241.

[25] Song JB, Song KX, Wei JS, *et al*. Microstructure characteristics and microwave dielectric properties of calcium apatite ceramics as microwave substrates. *J Alloys Compd* 2018, **731**: 264–270.

[26] Bian JJ, Song GX, Yan K. Structure and microwave dielectric properties of $Ba_{1+x}[(Co_{0.7}Zn_{0.3})_{1/3}Nb_{2/3}]O_3$ ($-0.015 \leqslant x \leqslant 0.015$). *J Eur Ceram Soc* 2007, **27**: 2817–2821.

[27] George S, Sebastian MT. Synthesis and microwave dielectric properties of novel temperature stable high Q, $Li_2ATi_3O_8$ (A = Mg, Zn) ceramics. *J Am Ceram Soc* 2010,

93: 2164–2166.

[28] Gurevich VL, Tagantsev AK. Intrinsic dielectric loss in crystals. *Adv Phys* 1991, **40**: 719–767.

[29] Wang KG, Zhou HF, Liu XB, *et al*. A lithium aluminium borate composite microwave dielectric ceramic with low permittivity, near-zero shrinkage, and low sintering temperature. *J Eur Ceram Soc* 2019, **39**: 1122–1126.

[30] Kai C, Li CC, Xiang HC, *et al*. Phase formation and microwave dielectric properties of $BiMVO_5$ (M = Ca, Mg) ceramics potential for low temperature co-fired ceramics application. *J Am Ceram Soc* 2019, **102**: 362–371.

[31] Kim SS, Na HG, Kwon YJ, *et al*. Synthesis and room-temperature NO_2 sensing properties of Sb_2O_5 nanowires. *Met Mater Int* 2015, **21**: 415–421.

[32] Freer R, Azough F. Microstructural engineering of microwave dielectric ceramics. *J Eur Ceram Soc* 2008, **28**: 1433–1441.

[33] Pullar RC, Penn SJ, Wang XR, *et al*. Dielectric loss caused by oxygen vacancies in titania ceramics. *J Eur Ceram Soc* 2009, **29**: 419–424.

[34] Surendran KP, Sebastian MT, Mohanan P, *et al*. Effect of nonstoichiometry on the structure and microwave dielectric properties of $Ba(Mg_{0.33}Ta_{0.67})O_3$. *Chem Mater* 2005, **17**: 142–151.

[35] Zhang TW, Zuo RZ. Effect of Li_2O–V_2O_5 addition on the sintering behavior and microwave dielectric properties of $Li_3(Mg_{1-x}Zn_x)_2NbO_6$ ceramics. *Ceram Int* 2014, **40**: 15677–15684.

[36] Desu SB, O'Bryan HM. Microwave loss quality of $BaZn_{13}Ta_{2/3}O_3$ ceramics. *J Am Ceram Soc* 1985, **68**: 546–551.